Pharm Res (2013) 30:2512–2522
DOI 10.1007/s11095-012-0958-3

RESEARCH PAPER

Effects of Particle Size and Surface Modification on Cellular Uptake and Biodistribution of Polymeric Nanoparticles for Drug Delivery

Sneha A. Kulkarni • Si-Shen Feng

Received: 21 April 2012 / Accepted: 7 December 2012 / Published online: 12 January 2013

ABSTRACT

Purpose To investigate the effects of the particle size and surface coating on the cellular uptake of the polymeric nanoparticles for drug delivery across the physiological drug barrier with emphasis on the gastrointestinal (GI) barrier for oral chemotherapy and the blood–brain barrier (BBB) for imaging and therapy of brain cancer.

Methods Various sizes of commercial fluorescent polystyrene nanoparticles (PS NPs) (*viz* 20 50, 100, 200 and 500 nm) were modified with the d-α-tocopheryl polyethylene glycol 1,000 succinate (vitamin E TPGS or TPGS). The size, surface charge and surface morphology of PS NPs before and after TPGS modification were characterized. The Caco-2 and MDCK cells were employed as an *in vitro* model of the GI barrier for oral and the BBB for drug delivery into the central nerve system respectively. The distribution of fluorescent NPs after *i.v.* administration to rats was analyzed by the high performance liquid chromatography (HPLC).

Results The *in vitro* investigation showed enhanced cellular uptake efficiency for PS NPs in both of Caco-2 and MDCK cells after TPGS surface coating. *In vivo* investigation showed that the particle size and surface coating are the two parameters which can dramatically influence the NPs biodistribution after *intravenous* administration. The TPGS coated NPs of smaller size (< 200 nm) can escape from recognition by the reticuloendothelial system (RES) and thus prolong the half-life of the NPs in the blood system.

Conclusions TPGS-coated PS NPs of 100 and 200 nm sizes have potential to deliver the drug across the GI barrier and the BBB.

KEY WORDS biodegradable polymers: blood–brain barrier (BBB) · chemotherapeutic engineering · gastrointestinal barrier (GI barrier) · pharmaceutical nanotechnology

INTRODUCTION

In recent decades the application of nanoparticles (NPs) for medicine and more specifically for drug delivery has increased rapidly. The NPs of a range of materials such as polymers, lipids and inorganic etc. are undergoing investigations especially for cancer therapy (1–4). They are colloidal-sized particles, having the size in the range between 1 to 1,000 nm, and drug may be either encapsulated inside the nanoparticles or attached to their surface. The drug encapsulated NPs offer various advantages such as delivery of drug in the optimum dosage range i.e. increase therapeutic efficacy of the drug, reduce adverse effects and improve patient compliance. In addition, NPs suspension can also be injected directly into the systemic circulation without possible embolism (5–7). It is clear that the size and surface properties of the NPs are playing a major role in determining the *in vivo* fate of the particles. The opsonization and subsequent recognition by the macrophages are strongly correlated with the size as well as surface functionality of the particle (8).

The various barriers present in the body like gastrointestinal barrier (GI) for oral chemotherapy and blood brain barrier (BBB) for drug delivery into the central nerve system. Several

S. A. Kulkarni • S.-S. Feng
Department of Chemical & Biomolecular Engineering
National University of Singapore
Block E5, 02-11
4 Engineering Drive 4
Singapore 117576, Singapore

S. A. Kulkarni • S.-S. Feng
NanoCore, National University of Singapore
Block EA, 04-27, 9 Engineering Drive 1
Singapore 117576, Singapore

S.-S. Feng
Department of Bioengineering, National University of Singapore
Block EA, 05-12, 9 Engineering Drive 1
Singapore 117576, Singapore

S.-S. Feng (✉)
Nanoscience & Nanoengineering Initiative (NUSNNI) & NanoCore
National University of Singapore, Block E3, 05-29
2 Engineering Drive 3
Singapore 117581, Singapore
e-mail: chefss@nus.edu.sg

mechanisms have been found in governing the transportation of NPs across these barriers, which include paracellular passage (size < 50 nm)—particles "kneading" between epithelial cells, endocytosis uptake (size < 500 nm)—particles absorbed by entrecotes through endocytosis and the lymphatic uptake (size < 5,000 nm)—particles adsorbed by the M cells of the Peyer's patches (9). Generally, the drug carrying nanoparticles are either administrated orally or intravenously. In case of oral administration, it has been reported that polymeric nanoparticles less than 500 nm can cross the M cells in the Peyer's patches of the intestine and easily taken up by the lymphatic system thus overcome the presystemic hepatic metabolism and enhance the bioavailability of the drug (10–12). However, in case of *i.v.* administration, it has been demonstrated that particles larger than 200 nm size can activate the human complement systems, thus being most likely cleared by the Kupffer cells. The particles under 200 nm in diameter display decreased rate of clearance and thus attain an extended circulation time as compared with those of a larger diameter. This phenomenon may be explained by the fact that smaller particles display a surface with a small radius of curvature preventing the efficient binding of opsonins (13). However, it has also been reported that drug encapsulated magnetic nanoparticles having size less than 100 nm were cleared by rapid reticuloendotheial system (RES) (14). Thus the clearance of the majority of particles makes it difficult to direct significant amount of nanoparticles to a desired target. Nevertheless, the circulation time of the NPs of a designated size can be greatly increased by surface modification either by hydrophilic or amphiphilic surface modifiers (14). The circulation time of NPs can also be further prolonged by the reduced renal excretion due to their appropriate particle size which prevents glomerular filtration. Furthermore, the polymeric nanoparticles with size less than 200 nm have an increased blood circulation and thus they show the better targeting effect especially to brain (15). Lockman *et. al* proposed that the thiamine ligand attached polymeric NPs having size less than 100 nm could be used to overcome BBB (15). It has been also demonstrated that polysorbate 80-coated polybutylcyanoacrylate nanoparticles could be used to overcome BBB especially for those of diameter below 100 nm. For the successful delivery of any drug to its targeted site, various factors such as its size, biocompatibility, target specific affinity, stability in blood and controlled drug release are needed to be considered during the synthesis of the nanoparticles.

The objective of the present study is to investigate the effects of particle size of polymeric nanoparticles of a designated surface modification for drug delivery across the physiological drug barriers with emphasis on the gastrointestinal (GI) barrier and the blood–brain barrier (BBB). The surface modification was carried out especially with TPGS, due to its great advantages in nanomedicine like the high water solubility, emulsification efficiency and excellent cellular adhesion (16–20). The polystyrene NPs of the various designated standard sizes *viz* 25, 50, 100, 200 500 nm were chosen as the model samples because of their uniform size distribution, ease of detection, purity (lack of contamination), size relevance to the field of nanotechnology and commercial availability (17,21–23). The size and size distribution, surface morphology and surface charge of PS NPs before and after TPGS coating were characterized using laser light scatterings (LLS), field emission scanning electron microscopy (FESEM) and zeta potential measurements respectively. The Caco-2 cell line was employed as an *in vitro* model of the GI barrier for oral drug delivery. The Madin-Darby canine kidney (MDCK) cells were used as an *in vitro* model of the BBB due to the tight junctions formed in the cell culture and the over expression of the P-glycoprotein, the multi-drug efflux pump proteins, in their cellular membrane. They also exhibit similar morphological and antigenic cell markers found in cerebral endothelial cells and can achieve a reproducible transendothelial electrical resistance along with the permeability to sucrose of less than or equal to 0.5×10^{-6} cm/s, close to the *in vivo* situation (24–27). The cellular uptake efficiency was measured by the fluorescence microplate reader. The distribution of fluorescent NPs in the various organs was analyzed by the high performance liquid chromatography (HPLC).

MATERIALS AND METHODS

Materials

Fluorescent dye encapsulated polystyrene (PS) nanoparticles (1% fluorescent label) were purchased from Duke Scientific (CA, USA). In general, fluorescent loaded polymer nanoparticles were prepared by a single-emulsion method. In brief, 100 mg of polymer precursor and 0.5 mg (0.25% w/w of polymer) of fluorescent maker was dissolved in 2 ml EA. The polymer/solvent mixture was then added drop-wise to emulsifier solution (0.2%) while vortexing at high setting for 30–40 s. Subsequently, the solution was sonicated for 30–40 s, to create an oil-in-water emulsion and poured into 100 ml water under rapid stirring conditions, followed by stirring for 14–16 h to evaporate the organic solvent. The NPs were collected by centrifugation and washed three to four times with water (Mili-Q) to remove the excess of emulsifier (25). Vitamin E TPGS was obtained from Eastman (TN, USA). Phosphate buffered saline (PBS), Hank's balanced salt solution (HBSS), penicillin streptomycin solution; Trypsin-EDTA solution and Triton® X-100 were purchased from Sigma. The solvents ethyl acetate (EA, analytical grade), dichloromethane and acetonitrile were purchased from Merck (Stadt, Germany). Fetal bovine serum (FBS) was received from Gibco (Life Technologies, AG, Switzerland). Madin-Darby canine kidney (MDCK) epithelial cell line (CCL-34, passages 58–70), Caco-2 and Eagle's minimum essential medium (EMEM) were purchased from American Type Culture Collection (ATCC,

USA). Ultrapure water (Millipore, Bedford, MA, USA) was used throughout the experiment. All chemicals were used as received without further purifications.

Preparation of TPGS Coated PS NPs (PS-TPGS)

Surface of fluorescent polystyrene NPs Duke Scientific (CA, USA) of various standard sizes were modified by TPGS. One mg/ml NPs suspension was added in 0.5% of TPGS in PBS and incubated for overnight at 37°C. The nanoparticles were collected *via* centrifugation (5810R, Eppendorf, 11,000 rpm, 30 min, 4°C), washed with Millipore water to remove excessive TPGS attached onto the NPs. Thus obtained NPs were freeze dried for storage and their suspension was used for the animal experiments.

Nanoparticles Characterization

Particle Size, Polydispersity, Zeta Potential and Surface Morphology

Size, polydispersity and zeta potential of PS NPs with and without TPGS coating were measured by photon correlation spectroscopy (PCS) using Zetasizer (Nano ZS, Malvern Instruments, Malvern, UK). The value was recorded as an average of three measurements. The samples were analyzed after dilution with deionized water to a count rate of 100–300 kcp.

Surface Morphology

The shape and surface morphology of NPs were investigated by field emission scanning electron microscopy (FESEM, JSM-6700F, JEOL, Japan). For FESEM, the samples were fixed on the stub with a double-sided sticky tape and then coated with platinum layer, which was carried out by an auto fine coater (JEOL, Tokyo, Japan) for 30's.

In Vitro Release Study

In vitro release of fluorescent marker from PS NPs with and without TPGS coating was carried out in 1 mM PBS (pH 7.4) at 37°C using dialysis bag diffusion technique. The 0.1 mg/ml NPs suspension (in PBS, pH 7.4) was filled in a dialysis bag (MW cutoff: 1000) and incubated in 10 ml of PBS solution in an orbital shaker at a constant gentle shaking of 100 rpm at 37°C. The incubated suspension was collected at designated time intervals and equal volume of fresh PBS was compensated. Samples were lyophilized and then reconstituted in 2 ml ethyl acetate. The amount of fluorescence in each of the release samples was analyzed by HPLC. All the samples were carefully protected from light throughout the experimental procedure

Cell Uptake of NPs

The cellular uptake efficiency of the fluorescent PS NPs with and without TPGS coating was assessed by using the Caco-2 cells as an *in vitro* model of the GI barrier for oral drug delivery and the MDCK as an *in vitro* model of the BBB. The Caco-2 and MDCK cells were cultured in MEM and EMEM medium respectively. The medium was replenished every alternate until confluence was achieved. The cells were then washed with PBS and harvested with 0.1% Trypsin–EDTA solution.

For quantitative cellular uptake study, Caco-2 and MDCK cells were seeded into 96-well black plates (Costar, IL, USA) at 1×10^3 cells/well (0.1 ml), and after the cells reached 80% confluence, the medium was changed to the suspension of the fluorescent PS NPs with and without TPGS coating at 100 μg/ml NPs concentration in the various designated time period of 0.5 h, 1 h, 2 h and 4 h. The cellular uptake analysis was also carried out after 2 h incubations with standard fluorescent PS NPs of sizes 25, 50, 100, 200 and 500 nm with and without TPGS coating at NPs concentration 100 μg/ml at 37°C. Data represents mean ± SD, n=6. After incubation in a designated time period, the NP suspension in the testing wells was removed and the wells were washed with 0.1 ml PBS three times. Subsequently, 50 μl of 0.5% Triton X-100 (in 0.2 N NaOH) solutions was added into all wells to lyse the cells. Microplate reader (Genios, Tecan, Switzerland) was used to measure the fluorescence intensity from the NPs in the desired wells with excitation wavelength at 468 nm and emission wavelength at 508 nm. The cellular uptake efficiency was expressed as the percentage of the fluorescence of the testing wells over that of the positive control wells as follows

$$\frac{I_{obs} - I_{NC}}{I_{PC} - I_{NC}} \times 100\%$$

where I_{obs} is the observed fluorescence intensity; I_{PC} is the fluorescence intensity of positive control, and I_{NC} is the fluorescence intensity of negative control.

For the qualitative uptake study, Caco-2 and MDCK cells were seeded in the 4-well covered glass chamber (LAB-TEK, Nagle Nunc, IL) till 70% confluence. The fluorescent NPs dispersed in the cell culture medium at concentration of 100 μg/ml were added into the wells. Cells were washed three times after incubation for 2 h and then fixed by 70% ethanol for 20 min. The cells were further washed thrice by PBS and the nuclei were then counter stained by propidium iodide (PI) for 45 min. The fixed cell monolayer was finally washed thrice by PBS and observed by confocal laser scanning microscope (Nikon, Zeiss LSM 510, Germany CLSM). Two different control experiments were used to study the cellular uptake efficiency: the fluorescent dye released from the NPs under *in*

vitro conditions and the free standard fluorescent dye (coumarin-6). The latter was found to have a negligible solubility in water (2×10^{-8}) and hence difficult to be used as a 'control' in the *in vitro* experiments".

In Vivo Study

The animal experiment protocols were approved by the Institutional Animal Care and Use Committees (IACUC), Office of Life Science, National University of Singapore. *In vivo* measurements were carried out with male Sprague–Dawley rats of 100–150 g and 4–6 weeks old, which were supplied by the Laboratory Animals Centre of Singapore and were maintained at the Animal Holding Unit of National University of Singapore. The animals were held in air-conditioned facility, provided with standard food and filtered water. The NPs were diluted in normal saline containing 0.9% w/v NaCl to obtain an estimated injection volume of 1–1.5 ml. Animals were randomly assigned to ten groups with each of three rats, which received *via* the tail vein an intravenous injection of the fluorescent PS NPs suspension at 15 mg/kg body weight. All animals were observed for mortality, general condition and potential clinical signs. After 3 h of the intravenous injection, animals in each group were anaesthetized and the blood was cleared with the circulation by transcardiac perfusion with approximately 200 ml ringer's solution until the blood flowing become faint pink in color. Subsequently the tissues namely heart, kidney, liver, stomach, intestine, spleen, lungs and brain were collected and stored at −80°C prior to analysis. The tissues were freeze-dried, weighed and homogenized. After that, 30 mg organ for each was mixed with 300 μl PBS, followed by extraction with ethyl acetate. Upon centrifugation at 11,000 rpm for 25 min, the organic layer was transferred to a glass tube and evaporated under nitrogen at room temperature overnight. The residue was dissolved in 100 μl of the HPLC mobile phase (acetonitrile/water 60:40 (v/v)) by vortex followed by centrifuged and subsequently transferred to auto sampler vials containing limited-volume inserts (90 μl). Plasma samples were harvested by centrifugation at 1,500 for 10 min and stored at −80°C until analysis. Liquid–liquid extraction was performed prior to the HPLC analysis. Briefly, the plasma (500 μl) was mixed with 100 μl of 10 mM phosphate-buffered saline (pH 7.8). The fluorescence was extracted by ethyl acetate on a vortex-mixer for 90 s. For the HPLC analysis, the C-18 column was used and the mobile phase was delivered at a rate of 1.3 ml/min. Sample (20 μl) was injected and the column effluent was detected with a fluorescence detector (λ_{ex} 468 nm, λ_{em} 508 nm). The fluorescence intensity was then calibrated with the standard calibration curves. Standard calibration curves were prepared as follows. Excess tetrahydrofuran (2 ml) was added to standard NP suspensions (25, 50, 100, 200 and 500 nm, 1 ml each) until clear solutions were obtained. The mixtures were allowed to evaporate to dryness. To ensure all the fluorescent labels were released, another excessive amount of dichloromethane was added to form clear solutions and allowed to evaporate until dryness. Acetonitrile (1.0 ml) was then added to these residuals and vortex dissolved. The acetonitrile solutions were then analyzed using HPLC with a fluorescence detector. The brain tissue sample for fluorescence microscopy imaging was prepared as per the procedure described in detailed in our earlier studies (25).

Statistical Analysis

Results were given as mean ± standard deviation (S.D). Mean values of nanoparticles size and total fluorescence content were compared using the Student's *t-test*. Differences are considered significant at a level of $P<0.05$.

RESULTS

Particle Size, Polydispersity Zeta Potential Analysis

The standard PS NPs used in the present work had uniform size of quite small polydispersity (Table I and Fig. 1). It can be seen from Table I that (1) the size of the fluorescent PS NPs was not significantly differing from their standard size; (2) the low polydispersity index clearly exhibits the monodispersed nature of the PS NPs; (3) the TPGS coating slightly increased both, the size and the polydispersity of the NPs; and (4) the high absolute value of the zeta potential implies the high stability of the NPs suspension. The mean diameter of the NPs was found to be increased after TPGS coating confirms the successful surface modification.

Morphology Study

The FESSM images of the fluorescent PS NPs of the various standard size further confirms that the NPs were monodispersed in nature (Fig. 1). Although the size of the PS NPs was observed to be slightly increased after TPGS coating, insignificant change in morphology was observed in the FESEM. The images were not included due to brevity.

In-Vitro Release

The *in vitro* release study of fluorescence PS and PS-TPGS NPs formulations were carried out to confirm that the fluorescence signal obtained during *in-vitro* as well as *in-vivo* analysis was mainly due to the uptake of NPs, instead of release fluorescence from the NPs in the medium. It was observed that fluorescence release for all types of the PS NPs was less than 3% after 4 h and less than 8% after 24 h. The data was not shown since it was insignificant and thus could be ignored.

Table I Particle Size, Polydispersity and Zeta Potential of Polystyrene Nanoparticles Before and After TPGS Coating

Std. PS NP size (nm)	Measured PS NP size (nm) (mean ± S.D[a]) and PI	Zeta potential (mV) (mean ± SD[a])	Size of PS NPs after TPGS coating (nm) (mean ± SD[a]) and PI	Zeta potential after TPGS coating (mV) (mean ± SD[a])
25	28.50 ± 1.86 (0.134)	−39.3 ± 2.1	33.11 ± 0.62 (0.138)	−27.3 ± 2.1
50	52.13 ± 1.10 (0.075)	−48.4 ± 3.2	65.76 ± 1.18 (0.157)	−32.7 ± 2.5
100	104.25 ± 0.07 (0.038)	−47.6 ± 1.8	113.40 ± 1.13 (0.090)	−30.2 ± 3.2
200	210.40 ± 5.09 (0.023)	−46.4 ± 2.4	222.00 ± 0.14 (0.015)	−26.7 ± 1.9
500	557.12 ± 0.07 (0.105)	−40.4 ± 1.5	580.13 ± 1.13 (0.193)	−25.5 ± 2.3

PS polystyrene

S.D standard deviation

PI Polydispersity Index

[a] $n=3$

Cellular Uptake

Effect of Particle Size

Figure 2 shows the cellular uptake efficiency of Caco-2 (a) and MDCK cells (b) after 2 h incubation with bare and TPGS coated PS NPs of different sizes at 37°C. It was clearly seen for the cellular uptake data that the PS NPs of sizes less than 200 nm were taken up by cells. The higher cellular uptake efficiency of Caco-2 cells was observed for the 100 nm size NPs as compared to other sizes (Fig. 2a). However, only small amount of PS NPs of 500 nm size was taken up by the cells. The uptake efficiency for all sizes of PS NPs was found to be increased after TPGS coating. Negligible cellular uptake efficiency was observed for the cells incubated with the fluorescent dye released from the NPs under *in vitro* conditions (data not shown).

Effect of Surface Coating, Incubation Time, and Temperature

It can be seen from Fig. 3 that a longer incubation time potentially leads to higher cellular uptake efficiency (up to 4 h). A significant rise in cellular uptake efficiency, (i.e. from 6.1% (1 h), 14.2% (2 h) to 15.33% (4 h)) was observed for the TPGS coated PS NPs.

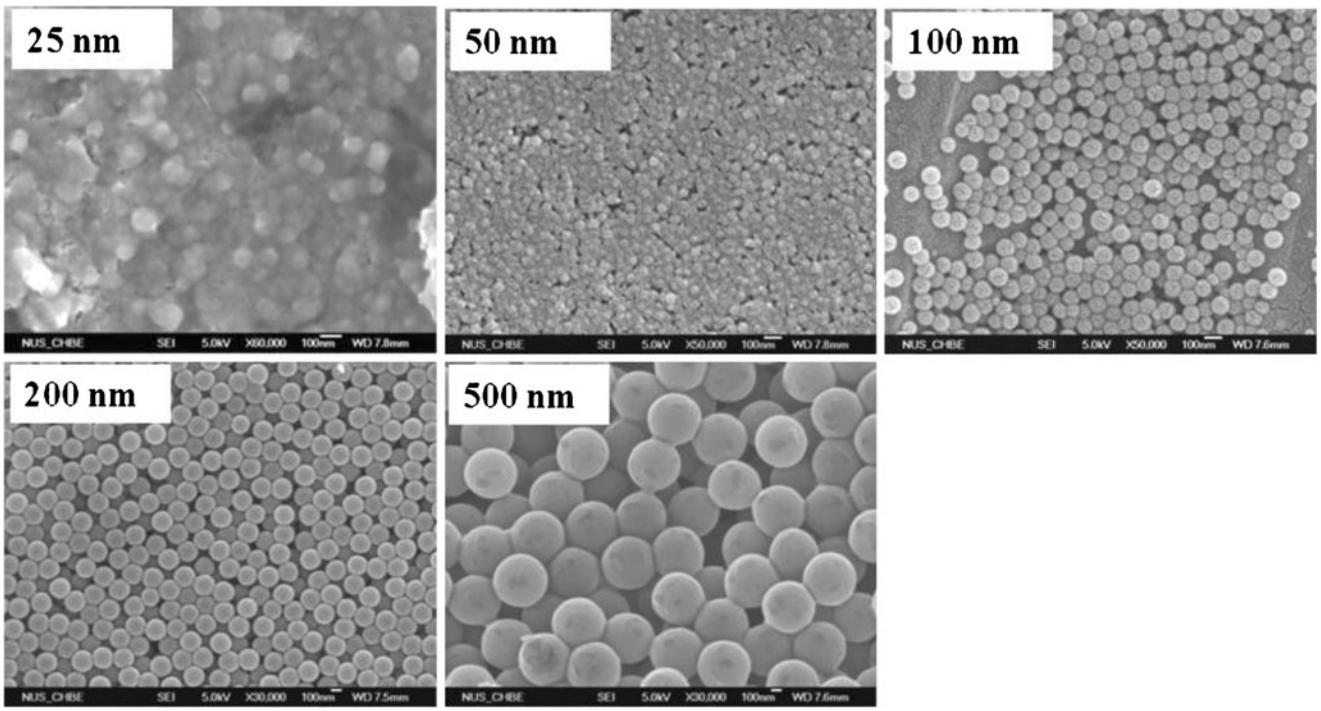

Fig. 1 Field emission scanning electron microscopic (FESEM) images of standard polystyrene nanoparticles of 25, 50, 100, 200 and 500 nm diameter in nominal sizes.

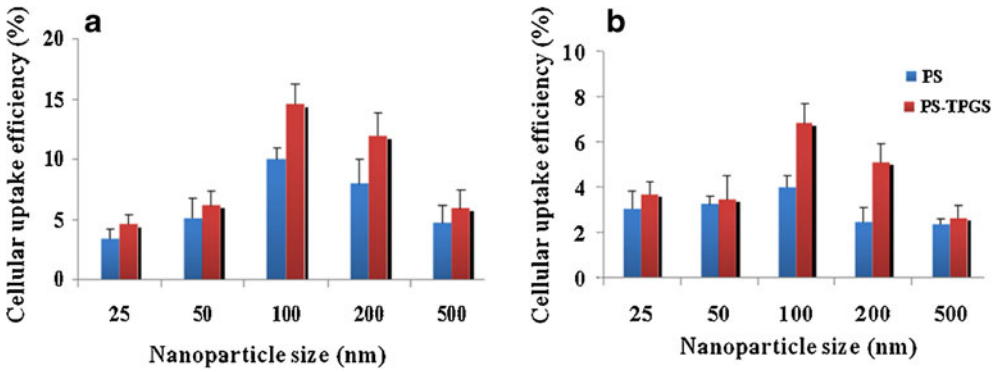

Fig. 2 Cellular uptake efficiency measurements of (**a**) Caco-2 and (**b**) MDCK cells after 2 h incubations with standard fluorescent polystyrene NPs of different sizes with and without TPGS coating at 37°C. NPs concentration: 100 μg/ml. Data represents mean ± SD, n=6.

Confocal microscopic images of the Caco-2 (a) and MDCK (b) cells were recorded after incubation with the different sized PS-TPGS NPs to support the quantitative nanoparticles uptake measurements described in the previous section (Fig. 4). The images were recorded by keeping the parameters such as sensitivity, gain, offset, and the laser power constant throughout the imaging process in order to compare the fluorescence intensity of the cells treated with various formations. The nucleus stained by propidium iodide (PI) was surrounded by green fluorescence clearly represent that TPGS coated NPs were internalized in the cytoplasm. In Fig. 4a, it can be clearly noticed that the fluorescence intensity in the cytoplasm of the cells incubated with 100 nm (column C) and 200 nm (column D) sized fluorescent PS-TPGS NPs were brighter than other cases. Interestingly, the MDCK cells incubated with the 25 (column A), 50 (column B) and 100 (column C) nm size PS-TPGS NPs exhibit a thicker layer of green fluorescence in the cytoplasm (Fig. 4b) as compared to the 200 (column D) and 500 (column E) PS-TPGS NPs. The Caco-2 and MDCK cell images taken after incubation with the various sizes bare PS NPs were not shown due to brevity.

In Vivo Analysis

Figure 5 shows the biodistribution among the various rat's organs (such as liver, spleen, lungs, kidney, heart, brain, intestine, stomach and blood) after 3 h of the *intravenous* injection of the various sized bare and TPGS coated fluorescent PS NPs suspension. It was observed that the TPGS surface coating had significant influence on the biodistribution of the PS NPs. It can be observed that (1) in general, higher concentration of fluorescence was seen in the liver and spleen tissues in comparison with the other organs; (2) the observed trends of the bare PS NPs distribution in the liver and spleen in accordance with NP sizes were 50 nm > 200 nm > 500 nm > 100 nm > 25 nm and 500 nm > 50 nm > 200 nm > 100 nm > 25 nm NPs respectively; (3) no distinction in the trend with respect to the NPs size was observed for distribution in the liver as well as in spleen. *Nevertheless*, significant decrease in NPs distribution in the liver and spleen was found for all sizes of NPs after TPGS coating (P<0.05). The amount of fluorescence associated with the blood plasma was seen to be increased with the PS-TPGS NPs in comparison with the bare PS NPs of the same particle size. For example, the concentration of the fluorescence associated with the PS-TPGS NPs was increased by a factor 8.8 and 4.1 in comparison with the nude PS NPs of the same 50 and 100 nm size, respectively. The distribution of the NPs in the lungs was found to be deceased after coating with TPGS. The higher distribution of the 500 nm nude PS NPs was found in the kidney. While, for PS-TPGS NPs, the distribution for all sized NPs in these organs for NPs excretion was found to be decreased and no prominent difference was observed among the PS-TPGS NPs of the various sizes. Similarly, in the heart, insignificant variation in the fluorescent concentration with respect to particle size was observed for the nude PS NPs, in contrast, the distribution of PS-TPGS NPs in the heart was observed to be increased.

Figure 6 illustrates the amount of the various NPs in the brain tissues after 3 h *intravenous* injection of the PS NPs suspension before and after TPGS coating. Interestingly, the

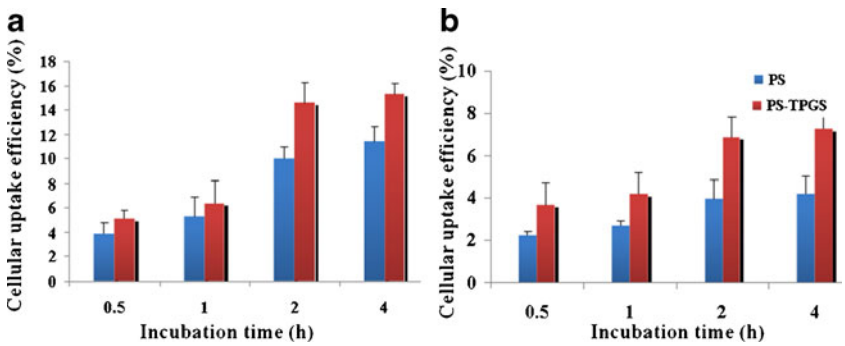

Fig. 3 The Caco-2 (**a**) and MDCK (**b**) cell uptake efficiency measurement after 0.5, 1, 2 and 4 h incubation with fluorescent PS nanoparticles of 100 nm diameter with and without TPGS surface coating at 37°C. NPs concentration 100 μg/ml. Data represents mean ± SD, n=6.

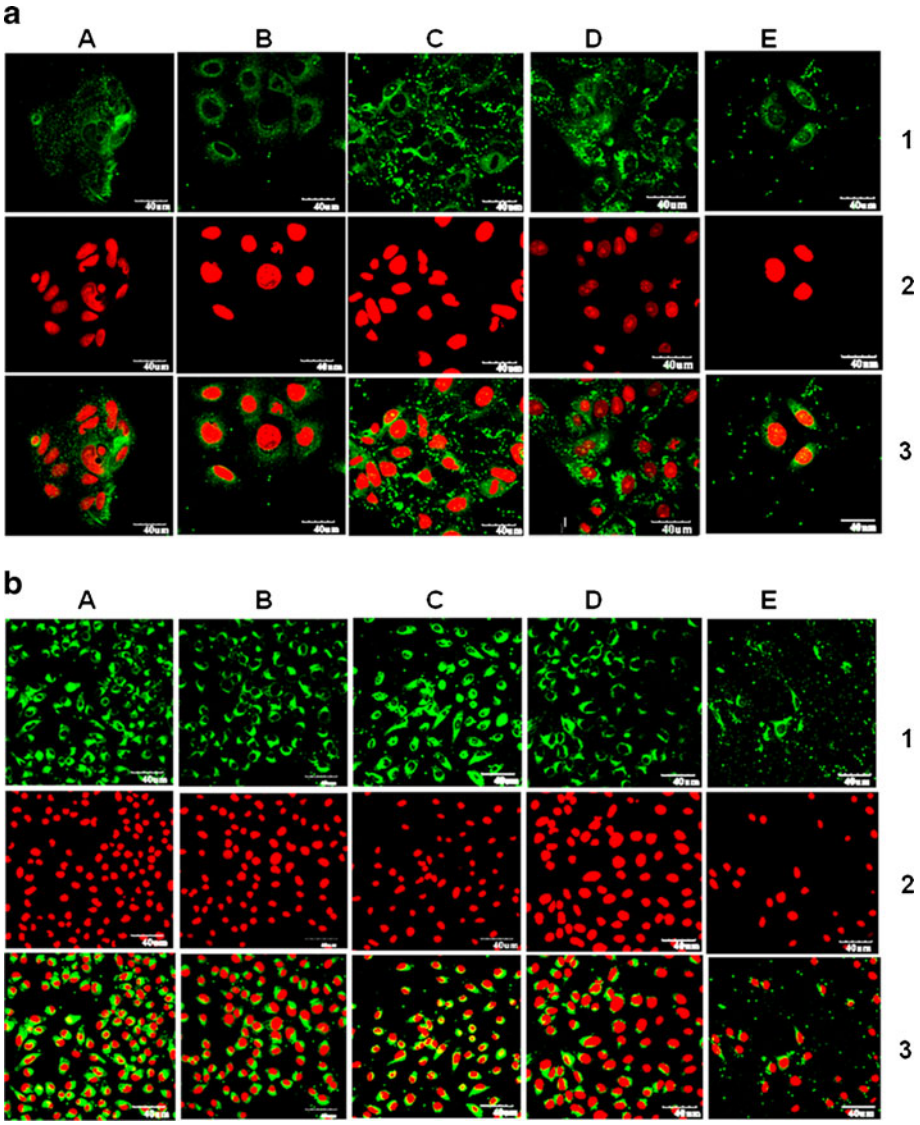

Fig. 4 Confocal laser scanning microscopy (CLSM) images of Caco-2 (**a**) and MDCK (**b**) cells after 2 h incubation with the fluorescent TPGS coated PS NPs. NPs concentration of 100 μg/ml. Column *A*, *B*, *C*, *D* and *E* are for the 25, 50, 100, 200 and 500 nm sized PS-TPGS NPs formulations respectively. Row 1: FITC channels showing the green fluorescence from PS NPs distributed in cytoplasm. Row 2: PI channels showing the red fluorescence from propidium iodide stained nuclei. Row3: Merged channels of FITC and PI. Scale bar = 40 μm.

observed trend of NPs distribution in the brain tissues was in the order of NPs size as 25>50>100>500>200 nm. The amount of the NPs across the BBB was further increased by the TPGS surface coating. Compared with the PS NPs, the PS-TPGS NPs were found about 2.4-, 1,7-, 1.4-, 1.1-, and 1.1- fold more in the brain tissues for these NPs of 25, 50, 100, 200 and 500 nm in diameter respectively.

It should be pointed out that the *in vivo* study is based on organs and thus much more complicated than the *in vitro* study based on cells. It is hardly to expect any direct correlation between them.

DISCUSSION

Commercially available fluorescent polystyrene (PS) NPs of the various designated standard sizes were used as model nanoparticles because of their uniform size distribution. The zeta potential was shifted towards more positive direction after surface coating. It may be due to positive charge of the adsorbed surface layer which was probably masking the surface charge of the NPs and force shear plane further away from surface of the NPs hence reducing the zeta potential relative to Stern potential (28). The TPGS was coated on the NPs surface by physical adsorption, which is a simple approach that provides stability to the NPs suspension as well as sustains their bioactivity. The higher cellular uptake efficiency was observed for the 100 nm size particles as compared to other sizes (Fig. 2). The size of the NPs plays a key role in their adhesion to and interaction with the biological cells and particles of 100–200 nm size can be best internalized by receptor-mediate endocytosis, while larger particles have to be taken up by phagocytosis (29–31). Also if the nanoparticles are too small, their surface energy would not be enough for the needed bending energy in the endocytosis process. Moreover, too small nanoparticles would result into small

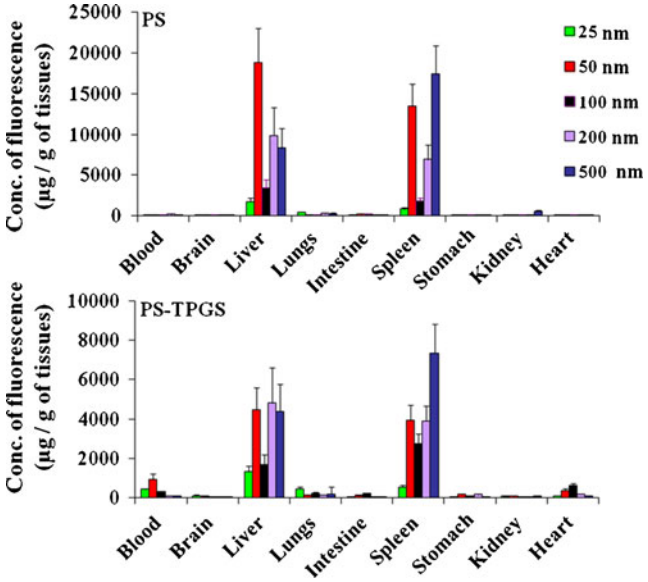

Fig. 5 Biodistribution of the fluorescent polystyrene nanoparticles of the various particle size for bare and TPGS coated PS NPs among the various organs (*µg/g*) of Sprague–Dawley rats 3 h after intravenous administration of PS NP formulations. The particle size is in nm. The NPs dose used is15 mg/kg. Data represents mean ±SD, *n*=3.

encapsulation efficiency and too fast drug release and therefore would not be preferred. It should be pointed out that the control experiments performed by incubating cells with

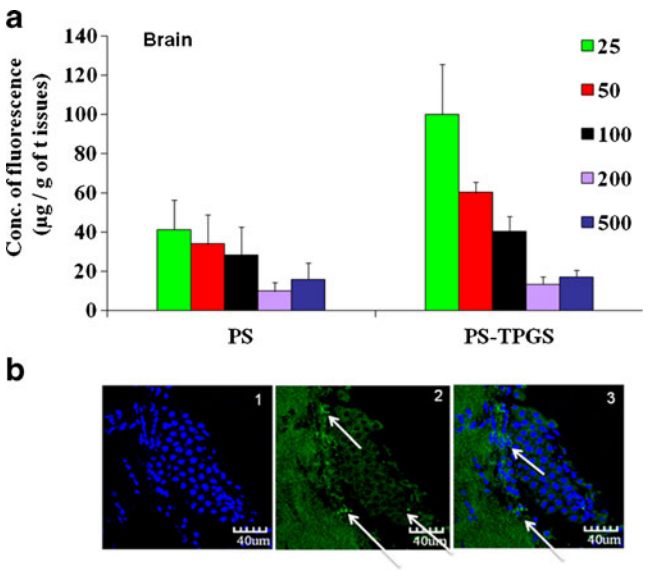

Fig. 6 (**a**) Biodistribution of the fluorescent polystyrene nanoparticles of the various particle sizes for nude and TPGS coated NPs in the brain tissues (*µg/g*) of Sprague–Dawley rats 3 h after intravenous administration of NP formulations. The particle size is in nm. The NPs dose used is 15 mg/kg. Data represents mean ±SD, *n*=3. (**b**) Representative confocal laser scanning microscopy image of the brain tissues of rat after intravenous injection of PS-TPGS NPs (100 nm). *1*) The nuclei in blue fluorescence are stained with DAPI. *2*) Fluorescein isothiocyanate channels showing the green fluorescence from fluorescent PS-TPGS nanoparticles distributed in brain tissues cytoplasm. *3*) Merged channels of fluorescein isothiocyanate and DAPI. *Arrows* indicate the distribution of the green florescence associated with brain tissues.

medium of the fluorescent released from the NPs did not show any significant uptake (data not shown). Caco-2 cells showed remarkable cellular uptake efficiency in comparison with MDCK cells, suggesting that MDCK cells were more selective to foreign particles, akin to the BBB. A significant rise in cellular uptake efficiency was observed after 4 h (Fig. 3a) clearly suggests that the cells were saturated by the NPs after 2 h and any extensions in incubation time would not have lead to higher cellular uptake efficiency. This also supports the claim by Desai (31). The same observation was made in case of MDCK cells. An optimal NP size can be obtained to attain best effect in cellular uptake and surface coating can show further enhancement (17). The enhancement in cellular uptake efficiency after surface coating with TPGS was mainly attributed to the inhibition of P-gp mediated transport as well as increase in the absorption by enhancing solubility and permeability due to hydrophilic nature of TPGS.

The fluorescence intensity in the cytoplasm of the cells incubated with 100 nm sized fluorescent PS-TPGS NPs (column c) and 200 nm size (column d) PS-TPGS NPs were brighter than other cases. Thus the obtained results were also in good agreement with the qualitative measurements.

The in-vivo analysis of various sized bare and TPGS coated fluorescent PS NP clearly indicates the significant enhancement in the NPs distribution in the brain tissues after TPGS coating especially for the particles having size below 100 nm (Figs. 5 and 6).

It is well-known that the biological fate of the injected foreign particles would mainly depend on their interactions with the proteins in the blood plasma as well as on the cells. Particle size and surface properties such as charge, morphology, hydrophilicity and surface modification with targeting ligand functionalization are the major controlling factors for interactions with the biological milieu (32–35). In this study, the fluorescence concentration associated with the blood plasma was found to be greatly enhanced especially for those of 100 and 200 nm size fluorescent PS-TPGS NPs (Fig. 5). The blood clearance of the smaller nanoparticles (< 80 nm) was two times as slow as the larger particles (> 200 nm) (35). Thus it clearly suggests that the particle size and surface modification play a key role for a sustained PK and the NPs of 100–200 nm in diameter may result in the best effects to escape from recognition by the reticuloendothelial system (17). The RES mainly consists of the mononuclear phagocytic cells that circulate in the bloodstream and the matured cells i.e. macrophages that reside mainly in the lungs, liver and spleen (28). It is a major obstacle for sustained PK as well as for targeting of the NPs to other parts of the body after intravenous administration. It was reported that the surface modification of the NPs with such surfactant as PEO/PPO block copolymers alleviated the interactions with blood components and thus prolonged the NPs in the blood circulations (32). The uncoated NPs were rapidly cleared from the circulation system and

targeted to organs where the mononuclear phagocyte system (MPS) was mainly located such as liver and spleen. That's why the NPs showed higher distribution in the liver and the spleen despite the observed fluorescence concentration associated with blood was low for the uncoated large size particles. Illum *et al.* have also reported that poloxamer coated NPs exhibited the inhibitory effect on the RES uptake and get diverted away from the liver and spleen to other tissues (36). A significant decrease in NPs distribution in the liver and spleen was observed for all sized TPGS coated PS NPs. It clearly demonstrates that the TPGS coated PS NPs were most likely not captured by the RES. This was probably because of the lower affinity of the hydrophilic surface of the TPGS modified NPs towards the MPS, commonly responsible for the opsonization or fast clearance of particles from the body. Thus the reduced accumulation in these major metabolic organs could be due to the 'stealth' effect of the TPGS coated NPs as well as avoiding the opsonization by escaping the recognition of the MPS. TPGS coated NPs probably slow down the first-pass metabolism and efflux transport thus enhances the chances of targeted delivery. The green fluorescence associated with the brain tissues (Fig. 6) after intravenous injection of TPGS coated fluorescent PS NPs clearly gives evidence that the fluorescence associated with the brain tissues was due to the uptake of surface coated NPs, which were able to cross the BBB (25). This study suggests that smaller size particles (< 200 nm) after coating with TPGS can overcome the RES uptake for effective drug delivery application to other parts of the body. The possible reason may be that nanoparticles less than 200 nm might be more similar to low density lipoprotein (LDL) than the other sizes. Also, since receptor-mediated transcytosis existed, the smaller the particles size, it is easier for the nanoparticles to enter the vascular endothelial cells of the BBB by endocytosis.

It should be pointed out that the cross-BBB or GI-barrier capability may still vary when different types of polymeric NPs with varies size, coating materials, surface function groups, surface charge, etc. were employed. Hence, the conclusion made in this research may only valid specifically on PS-based polymeric nanoparticles with TPGS modification, let alone possible complexity gained when the NPs were really loaded the therapeutics or contrast agent. Also, the success of increase of MDCK and Caco-2 uptake does not represent the barrier-across capability *in vivo*.

DISCUSSION

It should be pointed out that although Caco 2 cells and MDCK cells have been used routinely as *in vitro* models in the study of drug delivery across the blood brain barrier (37–42), there are other cells such as brain endothelial cells or epithelia cells from choroid plexus and other brain capillary derived cells, which may better represent the BBB due to their cellular and molecular structure similar to that of the brain capillary endothelial cells (43–47). Nevertheless, none of them can be a perfect model since the results obtained from any *in vitro* model can only partially simulate the cellular and molecular structure of the BBB. *in vivo* experiments are absolutely needed to provide guidelines for further clinical trials.

As regards the mechanism for nanoparticles to deliver the payrolls across the BBB, there has been intensive theoretical and experimental investigation in the literature (48,49). Compared with paracytosis of drug molecules across the tight junctions of the brain capillary cells, endocytosis of nanoparticles have much higher efficiency in drug delivery across the BBB, which bring all drug molecules encapsulated in the nanoparticles across the BBB at a time. Recognition of the multidrug resistance efflux pump proteins in the BBB can also be avoided. The particle size and the surface functionalization may have decisive effects in the endocytosis process, in which the surface energy of the nanoparticles are sacrificed to overcome the bending energy needed for a small piece of the lipid bilayer to envelop the nanoparticles and bring them into the cytoplasm.

CONCLUSIONS

We have investigated the effects of the particle size and surface coating especially using TPGS on the cellular uptake of the polymeric nanoparticles for drug delivery across the physiological drug barrier with emphasis on the gastrointestinal (GI) barrier for oral chemotherapy and the blood–brain barrier (BBB) for imaging and therapy of brain cancer. The standard PS NPs used had uniform size of quite low polydispersity index although the TPGS coating slightly increased both, the size as well as the polydispersity of the nanoparticles. High absolute value of the zeta potential implied the high stability of the NPs suspension. *In vitro* fluorescence release study confirmed that the fluorescence signals obtained from *in-vitro* as well as *in-vivo* analysis were mainly because of the cell-associated fluorescent nanoparticles but not from fluorescence released from the NPs in the medium. The higher cellular uptake efficiency of Caco-2 as well as MDCK cells was observed for the 100 nm size NPs as compared to other sizes. A longer incubation time potentially leads to higher cellular uptake efficiency. *In vivo* investigation revealed that particle size and surface coating are the two parameters which can dramatically influence the NPs biodistribution after *intravenous* administration. TPGS-coated NPs of 100 and 200 nm sizes have potential to deliver the drug across the GI barrier and the BBB. It has been pointed out in the literature that although widely used, Caco 2 cells and MDCK cells may not be the best *in vitro*

models of the BBB. Instead, other primary culture cells such as brain endothelial cells and epithelia cells from choroid plexus may be closer to the BBB in structure and thus should be used as the *in vitro* model of the BBB in the further study on this topic. Moreover, *in vitro* experiments are far from the real case. Any conclusion drawn from *in vitro* experiment should be confirmed by *in vivo* experiment (24,50–52).

ACKNOWLEDGMENTS AND DISCLOSURES

This work is supported by the Singapore–China Cooperative Research Project between Agency of Science, Technology and Research (A*STAR), Singapore and Chinese Ministry of Science and Technology (MOST) (R-398-000-077-305, PI: Feng SS) and the NUS FSF grant R-397-000-136-731 and FRC grant (R-397-000-136-112, Co-PI: Feng SS). SAK would like to thank NanoCore for providing the postdoctoral fellowship. As well as Dr V. Gopal and Dr M.S. Muthu for valuable discussions and Mr C.W. Gan, Mr W.M. Phyo, Mr P. Chandrasekharan and Ms S.Y. Chaw for their kind help in experiments.

The authors report no conflict of interest.

REFERENCES

1. De Jong WH, Borm PJA. Drug delivery and nanoparticles: applications and hazards. Int J Nanomed. 2008;3:133–49.
2. Gref R, Minamitake Y, Peracchia M, Trubetskoy V, Torchilin V, Langer R. Biodegradable long-circulating polymeric nanospheres. Science. 1994;263:1600–3.
3. Labhasetwar V, Song C, Levy RJ. Nanoparticle drug delivery system for restenosis. Adv Drug Deliv Rev. 1997;24:63–85.
4. Sinha VR, Bansal K, Kaushik R, Kumria R, Trehan A. Poly-ϵ-caprolactone microspheres and nanospheres: an overview. Int J Pharm. 2004;278:1–23.
5. Feng S-S, Chien S. Chemotherapeutic engineering: application and further development of chemical engineering principles for chemotherapy of cancer and other diseases. Chem Eng Sci. 2003;58:4087–14.
6. Ahlin P, Kristl J, Kristl A, Vrečer F. Investigation of polymeric nanoparticles as carriers of enalaprilat for oral administration. Int J Pharm. 2002;239:113–20.
7. Cavalli R, Bargoni A, Podio V, Muntoni E, Zara GP, Gasco MR. Duodenal administration of solid lipid nanoparticles loaded with different percentages of tobramycin. J Pharm Sci. 2003;92:1085–94.
8. He C, Hu Y, Yin L, Tang C, Yin C. Effects of particle size and surface charge on cellular uptake and biodistribution of polymeric nanoparticles. Biomaterials. 2010;31:3657–66.
9. Florence AT, Hillery AM, Hussain N, Jani PU. Nanoparticles as carriers for oral peptide absorption: Studies on particle uptake and fate. J Control Release. 1995;36:39–46.
10. Melody AS. The physiology of the lymphatic system. Adv Drug Deliv Rev. 2001;50:3–20.
11. Lisa B-P. Recent advances on the use of biodegradable microparticles and nanoparticles in controlled drug delivery. Int J Pharm. 1995;116:1–9.
12. Peppas LB. Recent advances on the use of biodegradable microparticles and nanoparticles in controlled drug delivery. Int J Pharm. 1995;116:1–9.
13. Aggarwal P, Hall JB, McLeland CB, Dobrovolskaia MA, McNeil SE. Nanoparticle interaction with plasma proteins as it relates to particle biodistribution, biocompatibility and therapeutic efficacy. Adv Drug Deliv Rev. 2009;61:428–37.
14. Duguet E, Vasseur S, Mornet S, Devoisselle J-M. Magnetic nanoparticles and their applications in medicine. Nanomedicine. 2006;1:157–68.
15. Lockman PR, Oyewumi MO, Koziara JM, Roder KE, Mumper RJ, Allen DD. Brain uptake of thiamine-coated nanoparticles. J Control Release. 2003;93:271–82.
16. Mu L, Feng SS. A novel controlled release formulation for the anticancer drug paclitaxel (taxol®): Plga nanoparticles containing vitamin e tpgs. J Control Release. 2003;86:33–48.
17. Yin Win K, Feng SS. Effects of particle size and surface coating on cellular uptake of polymeric nanoparticles for oral delivery of anticancer drugs. Biomaterials. 2005;26:2713–22.
18. Mu L, Feng SS. Vitamin e tpgs used as emulsifier in the solvent evaporation/extraction technique for fabrication of polymeric nanospheres for controlled release of paclitaxel (taxol®). J Control Release. 2002;80:129–44.
19. Mu L, Feng SS. PLGA/TPGS nanoparticles for controlled release of paclitaxel: effects of the emulsifier and drug loading ratio. Pharm Res. 2003;20:1864–72.
20. Dintaman JM, Silverman JA. Inhibition of p-glycoprotein by d-α-tocopheryl polyethylene glycol 1000 succinate (tpgs). Pharm Res. 1999;16:1550–6.
21. Zauner W, Farrow NA, Haines AMR. *In vitro* uptake of polystyrene microspheres: effect of particle size, cell line and cell density. J Control Release. 2001;71:39–51.
22. Sundaram S, Roy SK, Ambati BK, Kompella UB. Surface-functionalized nanoparticles for targeted gene delivery across nasal respiratory epithelium. FASEB J Res Commun. 2009;23:3752–65.
23. Mahler GJ, Esch MB, Tako E, Southard TL, Archer SD, Glahn RP, *et al.* Oral exposure to polystyrene nanoparticles affects iron absorption. Nat Nanotechnol. 2012;7:1–8.
24. Wang Q, Rager JD, Weinstein K. Evaluation of the mdr mdck cell line as a permeability screen for the blood -brain barrier. Int J Pharm. 2005;288:349–59.
25. Kulkarni SA, Feng S-S. Effect of surface modification on delivery efficiency of biodegradable nanoparticles across the blood -brain barrier. Nanomedicine. 2011;6:377–94.
26. Cho MJTD, Cramer CT. The madin darby canine kidney (mdck) epithelial cell monolayer as a model cellular transport barrier. Pharm Res. 1989;3:71–7.
27. Veronsi B. Characterization of the mdck cell line for screening neuroxiciants. Neurotoxicology. 1996;17:433–43.
28. Hillery AM, Florence AT. The effect of adsorbed poloxamer 188 and 407 surfactants on the intestinal uptake of 60-nm polystyrene particles after oral administration in the rat. Int J Pharm. 1996; 132:123–30.
29. Foster KA, Yazdanian M, Audus KL. Microparticulate uptake mechanisms of *in-vitro* cell culture models of the respiratory epithelium. J Pharm Pharmacol. 2001;53:57–66.
30. Couvreur P, Puisieux F. Nano- and microparticles for the delivery of polypeptides and proteins. Adv Drug Deliv Rev. 1993;10:141–62.
31. Desai MP, Labhasetwar V, Walter E, Levy RJ, Amidon GL. The mechanism of uptake of biodegradable microparticles in caco-2 cells is size dependent. Pharm Res. 1997;14:1568–73.
32. Tan JS, Butterfield DE, Voycheck CL, Caldwell KD, Li JT. Surface modification of nanoparticles by peo/ppo block copolymers to minimize interactions with blood components and prolong blood circulation in rats. Biomaterials. 1993;14:823–33.

33. Tosi G, Vergoni AV, Ruozi B, Bondioli L, Badiali L, Rivasi F, *et al.* Sialic acid and glycopeptides conjugated plga nanoparticles for central nervous system targeting: *in vivo* pharmacological evidence and biodistribution. J Control Release. 2010;145:49–57.
34. Vergoni AV, Tosi G, Tacchi R, Vandelli MA, Bertolini A, Costantino L. Nanoparticles as drug delivery agents specific for cns: *in vivo* biodistribution. Nanomed Nanotechnol Biol Med. 2009;5:369–77.
35. Fang C, Shi B, Pei YY, Hong MH, Wu J, Chen HZ. *In vivo* tumor targeting of tumor necrosis factor-α-loaded stealth nanoparticles: effect of mepeg molecular weight and particle size. Eur J Pharm Sci. 2006;27:27–36.
36. Illum L, Davis SS. Effect of the nonionic surfactant poloxamer 338 on the fate and deposition of polystyrene microspheres following intravenous administration. J Pharm Sci. 1983;72:1086–9.
37. Navarro C, González-Álvarez I, González-Álvarez M, Manku M, Merino V, Casabó VG, *et al.* Influence of polyunsaturated fatty acids on cortisol transport through mdck and mdck-mdr1 cells as blood–brain barrier *in vitro* model. Eur J Pharm Sci. 2011;42:290–9.
38. Hombach J, Bernkop-Schnürch A. Chitosan solutions and particles: evaluation of their permeation enhancing potential on mdck cells used as blood brain barrier model. Int J Pharm. 2009;376:104–9.
39. Madgula VLM, Bharathi A, Reddy NVL, Khan IA, Khan SI. Transport of decursin and decursinol angelate across Caco-2 and MDR-MDCK cell monolayers. *In vitro* models for intestinal and blood–brain barrier permeability. Planta Medica. 2007;73(4):330–5.
40. Wang Q, Rager JD, Weinstein K, Kardos PS, Dobson GL, Li J, *et al.* Evaluation of the MDR-MDCK cell line as a permeability screen for the blood–brain barrier. Int J Pharm. 2005;288:349–59.
41. Bacon J, Clark H, Felke E. Validation of MDCK 1.23 cells as a blood–brain barrier model. 7th European ISSX Meeting Location: Vancouver, Canada Date: Aug. 29–Sep 02, 2004;36:101.
42. Wang Q, Rager, J, Li JB. Preliminary evaluation of MDR-MDCK as a permeability screen for the blood–brain barrier.12th North American ISSX Meeting Location: Povidence, Rhode Island Oct 12–16, 2003;35:157.
43. Freese C, Uboldi C, Gibson MI, Unger RE, Weksler BB, Romero IA, *et al.* Uptake and cytotoxicity of citrate-coated gold nanospheres: comparative studies on human endothelial and epithelial cells. Part Fiber Toxicol. 2012;9(23):1–11.
44. Dakwar GR, Hammad IA, Popov M, Linder C, Grinberg S, Heldman E, *et al.* Delivery of proteins to the brain by bolaamphiphilic nano-sized vesicles. J Control Release. 2012;160:315–21.
45. Agarwal A, Majumder S, Agrawal H, Majumdar SP, Agrawal G. Cationized albumin conjugated solid lipid nanoparticles as vectors for brain delivery of an anti-cancer drug. Curr Nanosci. 2011;7(1):71–80.
46. Jain A, Chasoo G, Singh SK, Saxena AK, Jain. Transferrin-appended PEGylated nanoparticles for temozolomide delivery to brain: *in vitro* characterisation. J Microencapsul. 2011;28(1):21–8.
47. Gao H-l, Pang Z-q, Fan L, Hu K-l, Wu B-x, Jiang X-g. Effect of lactoferrin-and transferrin-conjugated polymersomes in brain targeting: *in vitro* and *in vivo* evaluations. Acta Pharmacol Sin. 2010;31:237–43.
48. Georgieva JV, Kalicharan D, Couraud P-O, Romero IA, Weksler B, Hoekstra D, *et al.* Surface characteristics of nanoparticles determine their intracellular fate in and processing by human blood–brain barrier endothelial cells *in vitro*. Mol Ther. 2011;19(2):318–25.
49. Chang J, Jallouli Y, Kroubi M, Yuan X-b, Feng W, Kang C-s, *et al.* Characterization of endocytosis of transferrin-coated PLGA nanoparticles by the blood–brain barrier. Int J Pharm. 2009;379:285–92.
50. Madgula VLM, Avula B, Reddy NVL, *et al.* Transport of decursin and decursinol angelate across Caco-2 and MDR-MDCK cell monolayers: *in vitro* models for intestinal and blood–brain barrier permeability. Plania Medica. 2007;73:330–5.
51. Hombach J, Bernkop-Schnuerch A. Chitosan solutions and particles: evaluation of their permeation enhancing potential on MDCK cells used as blood brain barrier model. Int J Pharm. 2009;376:104–9.
52. Navarro C, Gonzalez-Alvarez I, Gonzalez-Alvarez M, *et al.* Influence of polyunsaturated fatty acids on Cortisol transport through MDCK and MDCK-MDR1 cells as blood–brain barrier *in vitro model. Eur J Pharm Sci. 2011;42:290–9.*